SUPPLEMENTARY MATERIALS

Section S1: Theoretical resolution and field-of-view analysis

Resolution

Collecting the intensity through MCF limits the system resolution due to both the diameter of the fiber, D, and the maximum accepted numerical aperture NA_{max} . Each core NA will limit the collected light to a maximum NA of NA_{max} for objects closer then $\frac{D}{2NA_{max}} - z_m$, i.e. $NA_{eff} = NA_{max}$. For objects at larger distances the NA will be limited by the bundle diameter to: $NA_{eff} = \frac{D}{2(z_o+z_m)}$. The theoretical diffraction-limited resolution of the system can thus be summed up as follows:

$$\sigma_x = \frac{\lambda}{2NA_{eff}} = \begin{cases} \lambda \frac{1}{2NA_{max}} & z_0 < \frac{D}{2NA_{max}} - z_m \\ \lambda \frac{(z_m + z_o)}{D} & z_0 \geq \frac{D}{2NA_{max}} - z_m \end{cases} \qquad \text{(S1)}$$

To validate this theoretical estimation and characterize the experimental system resolution, we performed a knife-edge measurement, where a sharp-edged reflective target was imaged (Fig. S3 A). The Point Spread Function (PSF) was calculated from the spatial derivative of the reconstructed target image for each image row, as shown in Fig. S3 A, B. The results for the obtained resolution as a function of the target distance, shown in Fig. 3J, are the FWHM of the calculated PSF averaged over the image rows. These are in very good agreement with the theoretical prediction, given in Eq.S1. The error-bars of Fig. 3J are the standard deviation of the PSF FWHM, calculated at the different rows.

Field of View

The theoretical Field of view (FOV) limitations of the system can be estimated from geometrical considerations: First, the object must be illuminated by the illumination field, which has an NA of the first mode of the MCF core (NA_1), i.e. $FoV \approx 2NA_1(z_o + z_m)$. For diffuse reflecting objects, this is the only limitation, and the spatial field of view can theoretically be larger than the MCF diameter, D. However, for specular targets that are parallel to the fiber facet, the reflection angle is similar to the incidence angle of the illumination light (neglecting the effects of diffraction), and light will be collected by the MCF only from reflectors that are located at a $FOV < \frac{D}{2}$. To sum up the theoretical considerations predict a FoV that is:

$$FOV = \begin{cases} \dfrac{D}{2} & for\ specular\ targets \\ 2NA_1(z_o + z_m) & for\ diffuse\ targets \end{cases} \qquad (S2)$$

As explained in the following section, the mirror distance in our experiments, z_m, is chosen such that $4NA_1 z_m \geq D$, resulting in $FOV \geq D/2$ for both specular and diffusive targets.

To validate the theoretical estimation and characterize the experimental system FoV, we characterized the FoV of the experimental system using a mirror as the imaged object. The mirror was reconstructed using digital back-propagation, but without normalizing by $|E_{illum}|$, leaving a Gaussian-like intensity profile. The diameter of the reconstructed intensity envelope can be used as a measure for the system FoV. As a figure of merit, we calculated the $1/e^2$-width of the reconstructed intensity profile. The result of these FoV measurements performed at multiple distances, are displayed in Fig.3I. They demonstrate an almost constant FoV at all distances, as theoretically expected. The practically useful FoV can be larger than this estimate since the exact definition of the FoV is dictated by the required signal to noise ratio (SNR), which is dependent on the illumination intensity and target reflectivity. In our experiments for imaging a reflecting USAF target using a $D = 650\mu m$ MCF, details of the target are clear at a FoV exceeding $300\mu m$ at all distances as shown in Fig. S3 C.

Each data point in Fig. 3I is the average $1/e^2$-width of the reconstructed image of the mirror, averaged at 6 different angles in a single reconstructed image, at intervals of 30 degrees. The error-bars in Fig. 3I are the standard deviation of the $1/e^2$-width at these 6 angles.

Section S2: Choice of optimal system parameters

Distal mirror distance

To choose the mirror distance, z_m, both the phase variation and the intensity profile of E_{ref} must be considered. First, the phase of the field is a spherical one, with a curvature of $2z_m$: $\phi\left(E_{ref}\right) = \frac{2\pi}{\lambda 4 z_m}(x^2 + y^2)$. To ensure a well-defined unvarying reference phase at each core, we demand that $d\frac{\partial}{\partial x}\phi\left(E_{ref}\right) \ll \pi$ over the entire distal facet. Differentiating the above expression for $\phi\left(E_{ref}\right)$, and plugging $x_{max} = D/2$ results in the following demand for the mirror distance:

$$z_m \gg \frac{Dd}{2\lambda} \qquad (S3)$$

In addition, the intensity profile must be wide enough to cover the entire fiber, i.e., requiring that $z_m \geq \frac{D}{4NA_1}$. The first requirement (eq. S3) automatically fulfills the latter, since $NA_1 \leq \frac{\lambda}{2d}$.

Distal mirror reflectively and reference- and signal-arms powers ratio

Three important system parameters affect the SNR of the measurements and can be determined by the demand to maximize the SNR of the system. First, the reflectively of the partially reflecting distal mirror, R, i.e., the power reflection coefficient. Second, the total illumination power emerging from the distal facet, P. The third parameter, A, is the fraction of the total illumination power which is in the reference arm. For the sake of simplicity, no absorption is considered, and an object with a total effective power reflection coefficient of $R_o \ll 1$ is considered. Where R_o also takes into account the power lost to propagation and effective reflective area of the object. For further ease of notations, we denote the power ratio in the object arm $B = 1 - A$, and the power transmission coefficient of the mirror $T = 1 - R$.

To analyze the optimal SNR, one may consider the signal collected by a single core. In each single core, four fields are superimposed, as described in "Suppression of spurious reflections" section. Using the same notations, we analyze the expected amplitude of each of them:

$$\begin{aligned} \left|E_{R,m}\right| &= \sqrt{PA}\sqrt{R} \\ \left|E_{R,o}\right| &= \sqrt{PA}\sqrt{T^2 R_o} \\ \left|E_{I,m}\right| &= \sqrt{PB}\sqrt{R} \\ \left|E_{I,o}\right| &= \sqrt{PB}\sqrt{T^2 R_o} \end{aligned} \qquad (S4)$$

Where $E_{R,m}$ and $E_{\mathrm{R,o}}$ are the reflections of the reference beam from the mirror and object, respectively. $E_{\mathrm{I,m}}$ and $E_{I,o}$ are the reflections of the illumination beam from the mirror and object, respectively.

The desired signal is the interference term between $E_{R,m}$ and $E_{I,o}$, while the constant background is proportional to all four intensities. Assuming the dominant source of noise in the camera detected signal is shot-noise from the strong background, as is commonly the case when using sCMOS cameras, the SNR in a single frame will be:

$$SNR \propto \frac{\left|E_{R,m}E_{I,o}\right|}{\sqrt{E_{R,m}^2 + E_{R,o}^2 + E_{I,m}^2 + E_{I,o}^2}} = \sqrt{P} \cdot \sqrt{AB} \cdot \frac{\sqrt{RT^2R_o}}{\sqrt{R + T^2R_o}} \qquad (S5)$$

The SNR is thus a product of three terms: the first is the total illumination power, that is limited in most practical applications by sample damage. The second term $\sqrt{AB} = \sqrt{A(1-A)}$ is maximized by setting $A = B = 0.5$, i.e., setting the powers in the two arms to be equal with a balanced MZI. Lastly, the third term in eq. S5 is maximized by setting R and T to fulfill:

$$\begin{aligned} \frac{R^2}{T^3} &= \frac{R_o}{2} \\ \Rightarrow R &\approx \sqrt{R_o/2} \end{aligned} \qquad (S6)$$

The last approximation is valid only assuming $R \ll 1$, which is indeed the case when considering weakly-reflecting objects. For example, for $R_o = 0.02$, equation S6 yields $R \approx 0.1$. In our experiments R is determined in the mirror fabrication process. For the results shown throughout this article, $R \approx 0.12$ was achieved by evaporating 10_{nm} of titanium on a microscope slide. To fine-tune the power ratio of the two arms, A, a polarizing beam-splitter along with two half-wave-plates was incorporated into the setup, as explained in the "Experimental design" section.

Fiber parameters

Commercial MCFs are characterized by several important parameters: the pitch, p, the single core NA, the number of modes in a single core, the total fiber diameter, D, and the intracore crosstalk. To use FiDHo, the correct fiber and mirror distance must be chosen. First, to maximize resolution, a large NA_{max} is needed, as achieved with larger core sizes. In addition, increasing the bundle size D will increase both NA_{eff} at larger angles and the FOV for weakly scattering targets, at the price of a larger footprint. Smaller pitch will improve resolution, since less spatial interpolation will be needed on the fiber facet. Lastly, to reduce bending sensitivity and to increase resolution, a fiber with minimal crosstalk should be chosen, while maintaining a reasonable fill factor. For the fibers and laser used throughout this article FIGH-06-300S, $D = 270\mu m$,$NA_{core} \sim 0.3$, and a subset of Schott 1533385,$D = 650\mu m$, $NA_{core} \sim 0.3$, $\lambda = 640\ nm$. In all experiments, a mirror distance of $z_m = 2000\mu m$ was used.

Fig. S1

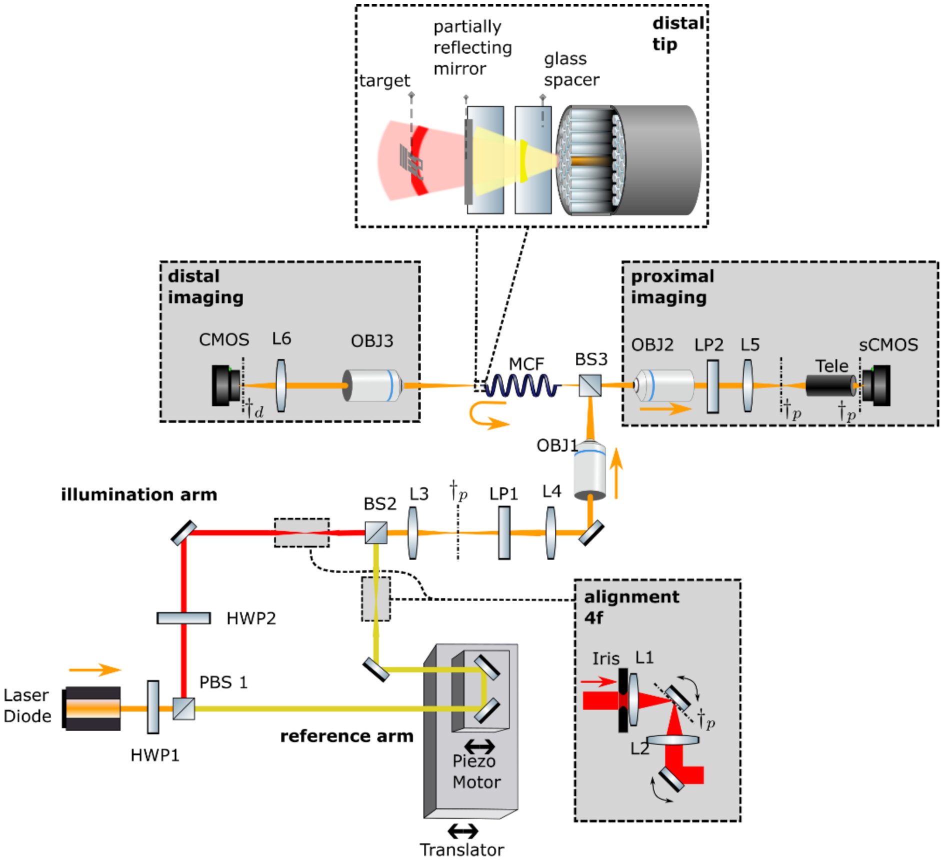

Fig. S1. Experimental setup. See section " Experimental Design " for complete description. HWP half-wave plate, PBS polarizing beam-splitter, BS beam-splitter, L lens, OBJ objective, MCF multicore fiber, Tele telescope, $\dagger_p, \dagger_d$ mark the proximal and distal conjugate planes, respectively.

s

Fig. S2

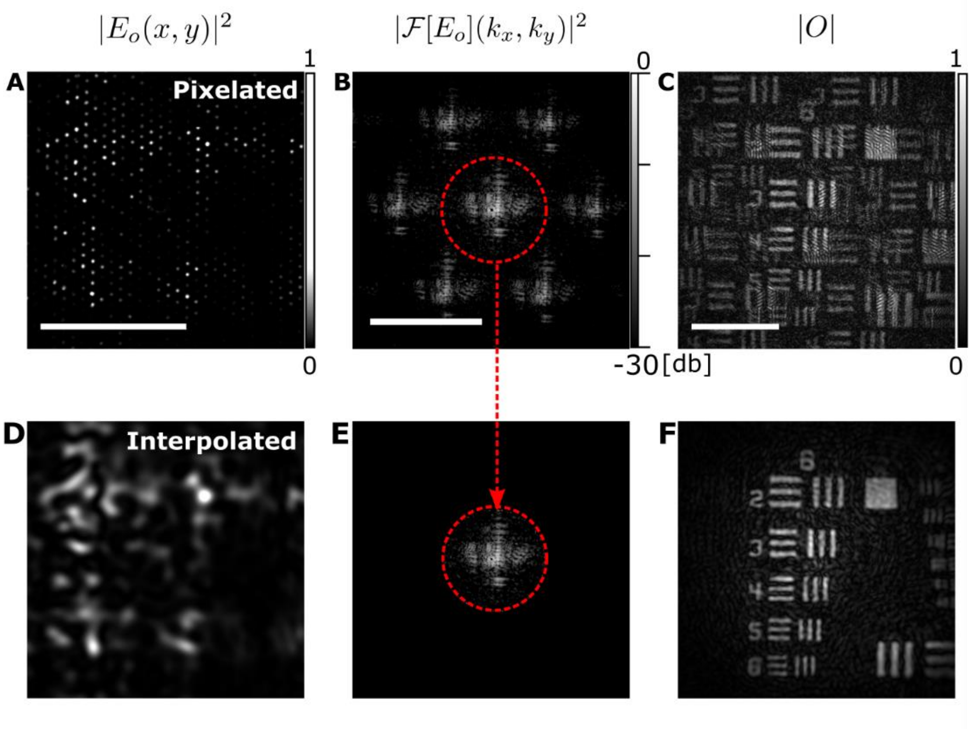

Fig. S2. Fourier Interpolation on ordered MCF (**A**) The retrieved distal field on a Schott fiber used throughout the article, shows the individual cores with a constant inter-core pitch. (**B**) In the frequency domain, clear replicas appear due to ordered sampling of the field. The red circle marks the frequencies to be saved. (**C**) Reconstruction of the object with no interpolation, shows ghosting of the object, due to aliasing. (**D, E, F**) show the same data, after filtering out higher spatial frequencies. Scale bars: A, C - $100_{\mu m}$ B - $\frac{2\pi}{pitch}$

Fig. S3

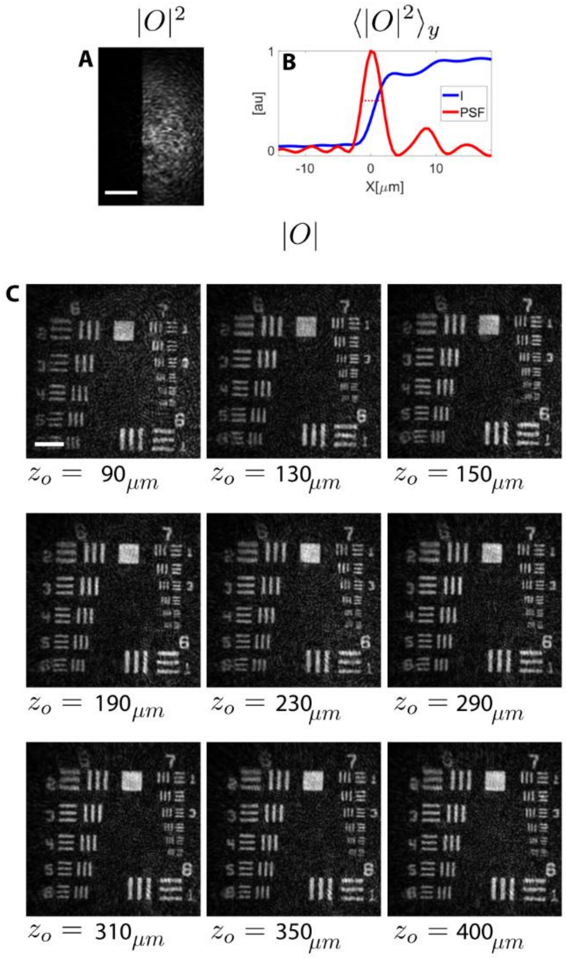

Fig. S3. Resolution and field-of-view characterization, detailed figure (**A**) a single image of the knife-edge mirror, using the edge of a USAF group 3 square, at a distance of $z_0 = 280\mu m$ (**B**) The mean cross section of (**A**)(blue), and the PSF (red) calculated as the spatial derivative of the cross section (red). The FWHM of the PSF, is indicated by the dashed line. (**C**) Imaging a USAF target at different depths, demonstrate the constant resolution and field of view. Scale bars: $50\mu m$

Fig. S4

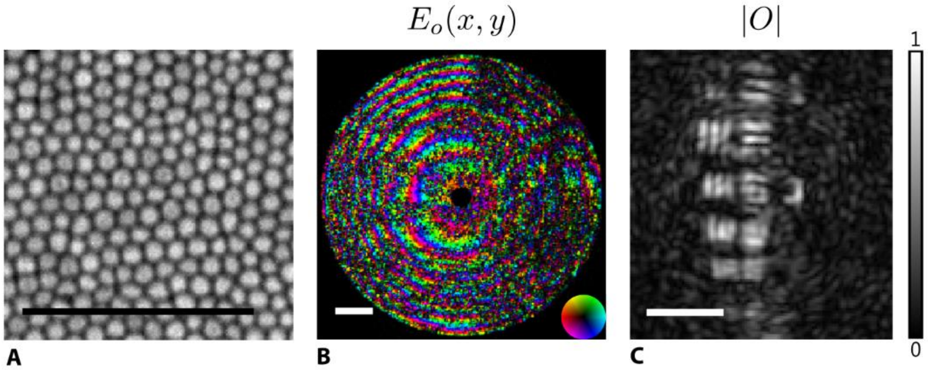

Fig. S4. Imaging using a disordered MCF (**A**) White light image of the FIGH-06-300S Fujikura fiber used (**B**) The retrieved distal field on the same fiber, when placing a reflective USAF resolution target at a distance of $z_0 = 100\mu m$ with the mirror placed at $z_m = 2_{mm}$. The cores are indiscernible due to binning of the camera pixels (**C**) The reconstructed object amplitude. Scale bars $40\mu m$.